Full-field absolute phase measurements in the heterodyne interferometer with an electro-optic modulator

Y. L. Chen*, H. C. Hsieh, W. T. Wu and D. C. Su
Department of Photonics and Institute of Electro-Optical Engineering,
National Chiao Tung University, 1001 Ta-Hsueh Road, Hsinchu 30050, Taiwan

ABSTRACT

A novel method for full-field absolute phase measurements in the heterodyne interferometer with an electro-optic modulator is proposed in this paper. Instead of the commonly-used half-wave voltage to drive the electro-optic modulator, a saw-tooth voltage signal with the amplitude being lower than its half-wave voltage is used. The interference signals become a group of periodical sinusoidal segments. The initial phase of each sinusoidal segment depends on the phase difference induced by the test sample. In real measurements, each segment is taken by a fast camera and becomes discrete digital points. After a series of operations, the starting point of the sampled sinusoidal segment can be determined accurately. Next, the period of the sampled sinusoidal segments is lengthened and they can be modified to a continuous sinusoidal wave by using a least-square sine fitting algorithm. The initial phase of the continuous sinusoidal wave can also be estimated. Subtracting the characteristic phase of the modulator from the initial phase, the absolute phase measured at the pixel can be obtained without the conventional reference signals. These operations are applied to other pixels, and the full-field absolute phase measurements can be achieved. The phase retardation of a quarter-wave plate is measured to show the validity of this method.

Keywords: electro-optic modulator, phase measurement, heterodyne interferometer

1. INTRODUCTION

In the heterodyne interferometry [1-6], the measured absolute phase is the phase difference between the test signal and the reference signal. In general, the reference signal can be obtained with a light signal from a beam-splitter or an electronic signal directly from an electronic device. However, as this technique extends to the full-field measurements, a camera is needed to grab the test signals and discrete digital signals in a limited exposure time are taken. Because they have an uncertain time difference with respect to the commonly-used reference signals, it is difficult to measure the full-field absolute phases using heterodyne interferometry. Although several papers [7-10] have reported how to tackle this problem, all of them can only measure the relative phases with the exception of Akiba's method [10]. Due to the usage of a pair of cameras, it is difficult to make the two images match each other very well.

In this paper, an alternative method for full-field absolute phase measurements in the heterodyne interferometer with an electro-optic modulator is proposed. An electro-optic modulator is used to introduce a frequency difference between two orthogonal polarizations in the heterodyne interferometer [11]. When the electro-optic modulator is applied with a saw-tooth voltage signal with the amplitude lower than its half-wave voltage, periodical sinusoidal segments are obtained. In the full-field measurements, the segments at every pixel are taken by a camera and become discrete digital signals. After a series of calculations, the starting point of the sinusoidal segment can be determined accurately. Next, the difference between the period of the saw-tooth signal and that of the periodical sinusoidal segments is inserted into any two consecutive segments. Thus the periodical sinusoidal segments have the same frequency as that of the applied saw-tooth signal. Then, the periodical sinusoidal segments can be modified as the periodical sinusoidal signals by using a least-square sine fitting algorithm [12]. Subtracting the initial phase of the system from the phase of the periodical sinusoidal signals, the absolute phase measured at the pixel can be obtained. This technique is applied to other pixels, and the full-field absolute phase measurements can be achieved. The validity of the technique is demonstrated.

*ylchen.eo94g@g2.nctu.edu.tw; phone +886-3-573-1951; fax +886-3-571-6631

Modeling Aspects in Optical Metrology II, edited by Harald Bosse, Bernd Bodermann, Richard M. Silver,
Proc. of SPIE Vol. 7390, 73900F · © 2009 SPIE · CCC code: 0277-786X/09/$18 · doi: 10.1117/12.828391

2. PRINCIPLE

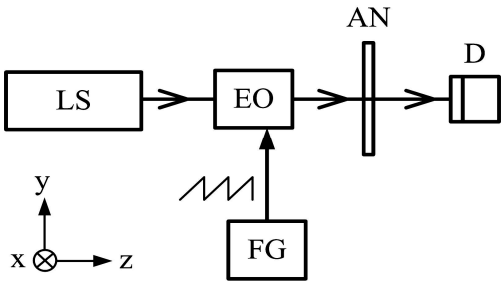

Fig. 1. Schematic diagram for measuring the interference signal of a heterodyne light beam: LS: laser light source; EO: electro-optic modulator; FG: function generator; AN: analyzer; D: photo detector.

Figure 1 shows a heterodyne light source with an electric-optic modulator. For convenience, the +z axis is chosen along the propagation direction and the y axis is along the vertical direction. A linearly polarized light at 45° with respect to the x-axis passes through an electro-optic modulator EO. If the fast axis of the EO is along the x axis, and an external sawtooth voltage signal with frequency f and amplitude V is applied to the EO, then the phase retardation between the s- and p- polarizations can be given as [13].

$$\Gamma = \Gamma_0 + \frac{\pi}{V_\pi} V_z , \tag{1}$$

where V_π is the half-wave voltage, and Γ_0 is the phase retardation without external field. In addition, V_z is the saw-tooth driving voltage and it can be expressed as

$$V_z(t) = \frac{2V}{T}\left(t - mT\right) + \left(V_\mathrm{b} - V\right), \tag{2}$$

where $mT \le t \le (m+1)T$, m is an integral, T (= $1/f$) and V_b are the period and the dc part of the saw-tooth voltage, respectively. Γ_0 can be zero with a moderate choice of V_b. Because V_b is a constant, it is omitted in this paper. Consequently, Eq. (2) can be rewritten as

$$\Gamma = \frac{V}{V_\pi}(2\pi f t - 2\pi m - \pi). \tag{3}$$

Let $V < V_\pi$, and we have

$$\Gamma = 2\pi f_0 t - \phi_0 ; \tag{4}$$

where

$$f_0 = (\frac{V}{V_\pi}) f , \tag{5}$$

and

$$\phi_0 = (\frac{V}{V_\pi})(2\pi m + \pi). \tag{6}$$

Both f_0 and ϕ_0 can be calculated under the experimental conditions that f, V and V_π are specified. It is obvious that f_0 is smaller than f.

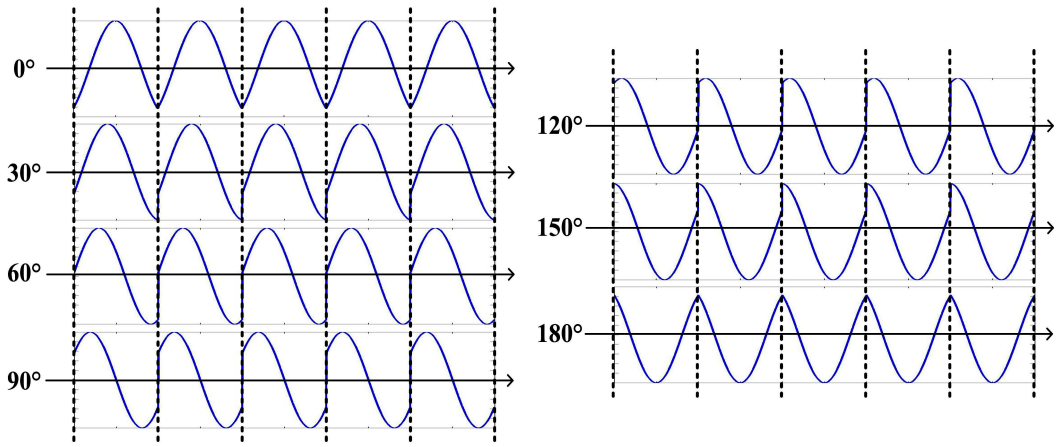

Fig. 2. Interference signals as ϕ is changed from 0° to 180° with 30° step under the condition V_π = 148 V and V = 120 V.

After the light passes through the analyzer AN at 45° with respect to the x-axis, the interference intensity in the m-th period (mT) is given as

$$I(t) = \frac{1}{2}[1+\cos(\Gamma)] = \frac{1}{2}[1+\cos(2\pi f_0 t - \phi_0)],\ mT \le t \le (m+1)T. \tag{7}$$

Because f_0 is smaller than f, Eq. (7) represents only a sinusoidal segment and not a sinusoidal wave with one cycle. This sinusoidal segment has breakpoints with its neighbor segments and its starting point depends on ϕ_m at m = 0 which can be regarded as the initial reference phase ϕ_0, that is

$$\phi_0 = \phi_m(m=0) = \frac{V}{V_\pi}\pi. \tag{8}$$

When an additional phase ϕ is introduced, the phase retardation becomes $\Gamma + \phi$. Consequently, the phase of the starting point is also shifted from ϕ_0 to $\phi_0 + \phi$. Hence, Eq. (7) can be rewritten in the continuous form as

$$I(t) = \frac{1}{2}\{[1+\cos(2\pi f_0 t - \phi_0 + \phi)]\cdot \mathrm{rect}[tf - 1/2]\} * \sum_{i=0}^{n-1}\delta[t - i/f]; \tag{9}$$

where the operator rect[ ] and the symbol * represent the rectangular function and the convolution operation, respectively. For clarity, the interference signals for several different ϕ can be depicted by substituting the following experimental conditions $V_\pi = 148$ V and $V = 120$ V into Eq. (9), and they are shown in Fig. 2. It is obvious that their starting points are different and depend on the associated ϕ.

The theoretical starting points of sinusoidal segments in the time axis are at local extreme positions, which can be determined by operating the second order differential on Eq. (9). They are always different from the starting points of the discrete digital signals taken by a camera, as shown in Fig. 3. The symbol • means the sampling positions. In theory, the ending point of one segment coincides with the starting point of the next segment. However, the discrete starting point of every segment may not be at the same relative position, and may not be at the starting position of the theoretical curve. To minimize the phase error, an "optimum segment" with a starting point being closest to the theoretical starting point is determined. Let P_m and C_m be the sampling starting point and the time comparing point of m-th segment, respectively. The initial condition $C_1 = P_1$ and the following rules are used as m = 1, 2, 3,… , i.

$$C_{m+1} = C_m + T, \quad \text{if } P_{m+1} > C_m + T; \tag{10-1}$$

$$C_{m+1} = P_{m+1}, \quad \text{if } P_{m+1} \le C_m + T. \tag{10-2}$$

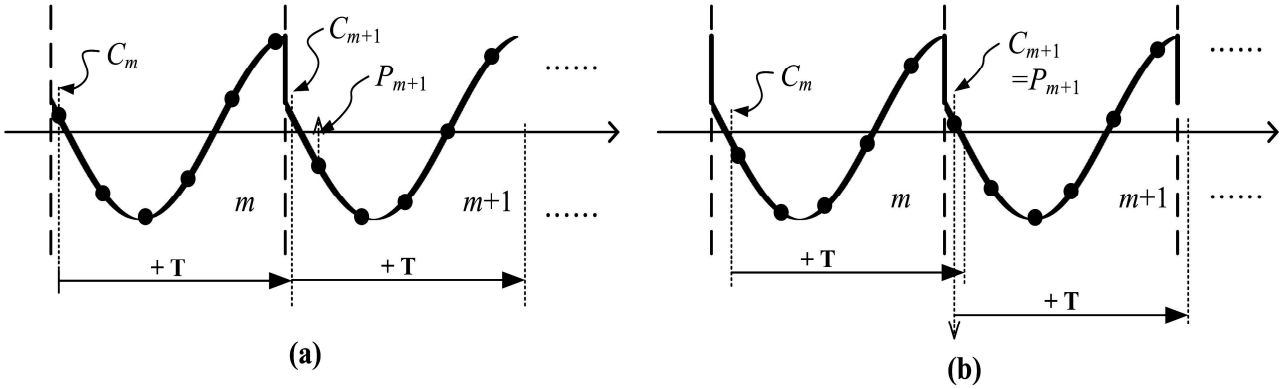

Fig. 3. The rules for identifying the optimum segment as (a) $P_{m+1} > C_m + T$, and (b) $P_{m+1} \le C_m + T$.

Fig. 3(a) and (b) show the conditions for Eqs. (10-1) and (10-2), respectively. If the *i*-th segment is the optimum segment, then the time axis is so shifted that the condition $P_i = 0$ is given and it can be written as

$$I_i(t) = \frac{1}{2}\{[1+\cos(2\pi f_0 t - \phi_0 + \phi)]\cdot \mathrm{rect}(f\,t - 1/2)\}\cdot \sum_{g=0}^{h-1}\delta\left(t - \frac{g}{f_s}\right), \tag{11}$$

where g is a positive integer, f_s and h are the sampling frequency and the number of sampled points in the *i*-th segment, respectively. Next, the period difference Δt, that is $\Delta t = 1/f_0 - 1/f$, is inserted into any two consecutive sampling segments as shown in Fig. 4. So the sampling segments have the same frequency f_0 as that of a certain sinusoidal wave. They and the phase $\phi - \phi_0$ of the starting point can be modified and estimated with the least-square sine fitting algorithm [12]. They become a continuously sinusoidal wave within the corresponding exposure time and can expressed as

$$I_c(t) = \frac{1}{2}[1+\cos(2\pi f_0 t - \phi_0 + \phi)]\cdot \tag{12}$$

The absolute phase ϕ can be calculated under the condition that ϕ_0 and $\phi - \phi_0$ are specified.

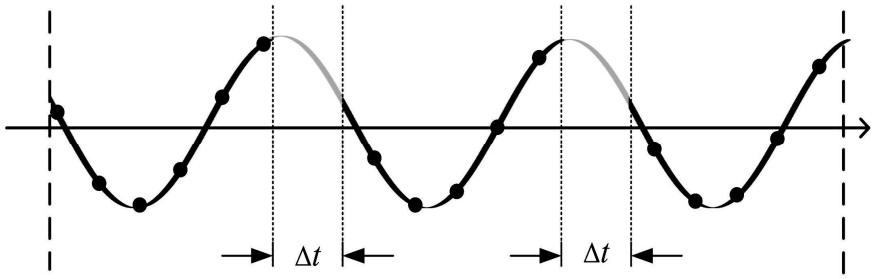

Fig. 4. Inserting Δt into any two consecutive segments.

3. EXPERIMENTS AND RESULTS

To demonstrate the feasibility of this method, an experimental schematic diagram of common-path heterodyne interferometer is designed and shown in Fig. 5 to measure the absolute 2D phase retardations of the sample. A linearly polarized light beam passes through an EO driven by a function generator (FG). A saw-tooth signal with frequency *f* and driving voltage lower than the half-wave voltage is applied the EO. The light beam is collimated by an optical module that consists of a microscopic objective (MO), a pinhole (PH), and a collimating lens (CL). Next, the collimated light passes through a test sample (S), an analyzer (AN), an imaging lens (IL), and finally enters a CMOS camera (C).

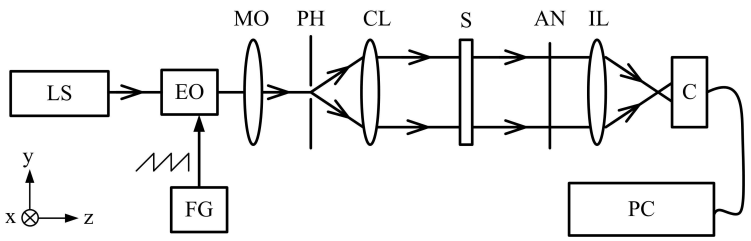

Fig. 5. Schematic diagram for measuring the full field phase retardations: LS: laser light source; EO: electro-optic modulator; FG: function generator; MO: microscopic objective; PH: pinhole; CL: collimating lens; S: sample; AN: analyzer; IL: imaging lens; C: CMOS Camera; PC: personal computer.

Let the laser light be linearly polarized at 45° with respect to the x-axis and both the fast axes of EO modulator and the S be along the x-axis, then the Jones vectors of the light amplitude on C can be derived as [14].

$$E_t = AN \cdot S \cdot E_o = \frac{1}{2}\begin{pmatrix} 1 & 1 \\ 1 & 1 \end{pmatrix}\begin{pmatrix} e^{i\frac{\phi}{2}} & 0 \\ 0 & e^{-i\frac{\phi}{2}} \end{pmatrix}\frac{1}{\sqrt{2}}\begin{pmatrix} e^{\frac{i\Gamma}{2}} \\ e^{-\frac{i\Gamma}{2}} \end{pmatrix} e^{i\omega_o t} = \frac{1}{2\sqrt{2}}\begin{pmatrix} e^{i\left(\frac{\Gamma+\phi}{2}\right)} + e^{-i\left(\frac{\Gamma+\phi}{2}\right)} \\ e^{i\left(\frac{\Gamma+\phi}{2}\right)} + e^{-i\left(\frac{\Gamma+\phi}{2}\right)} \end{pmatrix} e^{i\omega_o t}. \tag{13}$$

Its intensities can be expressed as

$$I_t = \frac{1}{2}[1 + \cos(\Gamma + \phi)] = \frac{1}{2}[1 + \cos(2\pi f_0 t - \phi_0 + \phi)]. \tag{14}$$

Because Eq. (14) is the same as Eq. (12), the absolute phase retardation ϕ can be measured by the method described in Section 2.

An He-Ne laser with 632.8 nm wavelength, an EO modulator (New Focus/Model 4002), and a CMOS camera (Basler/A504K) with 8-bit gray level and 200×200 pixel image resolution are used to test a transparent glass plate, a quarter wave-plate and a half wave-plate, respectively. Under the conditions f = 1 Hz, V_π = 148 V, sampling frequency f_s = 45.1 frames/sec, and 500 frames are taken. Here V = 120 V is chosen and we have ϕ_0 = 146°.

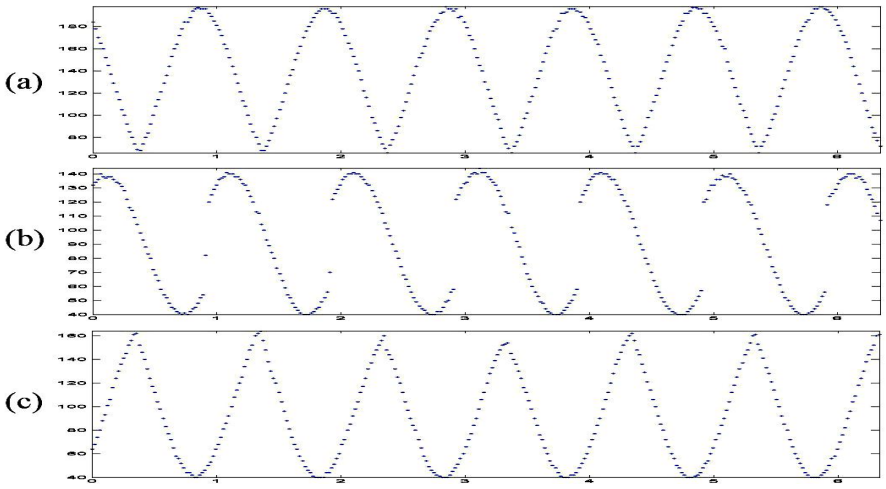

Fig. 6. The intensities of the sampling signals for the pixel at (+100, +100) for (a) a transparent glass plate, (b) a quarter-wave plate, and (c) a half-wave plate.

The intensities of the sampling signals for the pixel at (+100, +100) are shown in Fig. 6, and they are similar to the theoretical curves shown in Fig. 2. This method is applied to every pixel; the associated phase retardation can be

obtained. Fig. 7 shows the measured full-field phase retardation distribution of the quarter-wave plate, and its standard deviation is 0.7°. The average phase retardations of all the pixels for these three samples are also calculated. They are 359°, 89.9°, and 180°, respectively.

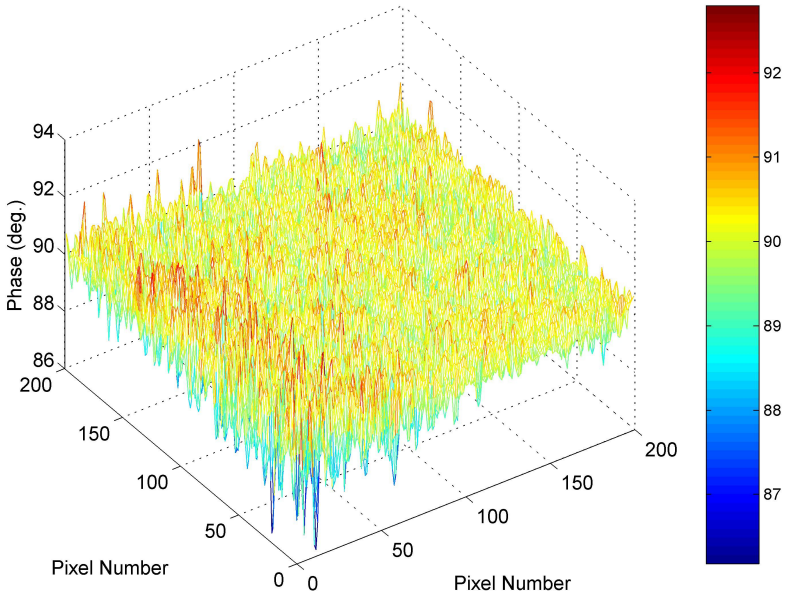

Fig. 7. The measured full-field phase retardation distribution of the quarter-wave plate.

4. DISCUSSION

For easy processing, the sinusoidal segment should be larger than the half cycle sinusoidal signal [15]; thus this method is valuable under the condition $(V_\pi / 2) < V < V_\pi$. The condition $V \approx (3V_\pi / 4)$ is chosen in our experiments. Moreover, if f_s is a multiple of f, then each segment has the same sampling points. Consequently, Equations (10-1) and (10-2) are not valid for determining the optimum segment. Under our experimental conditions, the errors in the absolute phase measurement in this technique may be influenced by the following four factors:

A. Characteristic phase error

The errors of the voltages V and V_π directly introduce a systematic error to the reference phase. The resolution of given voltage V from the power supplier is 0.0016 V. Also V_π can be measured [16] and its error is estimated $\Delta V_2 = 0.015$ V. Hence the maximum error of ϕ_0 can be estimated and expressed as $\Delta\phi_0 = \phi_{\max} \cdot \left[(\Delta V_1 / V)^2 + (\Delta V_2 / V_\pi)^2\right]^{1/2} \approx 0.03°$, where $\phi_{\max} = 180°$ is the maximum possible phase.

B. Sampling error

It depends on the frequency of the heterodyne interference signal, the camera recording time, the frame period, the frame exposure time, and the number of gray levels. The phase error from the sampling processes can also be estimated and it is given $\Delta\phi_s = 0.036°$ [17].

C. Polarization-mixing error

Owing to the extinction ratio effect of a polarizer, mixing of light polarization occurs. In our experiments, the extinction ratio of the polarizer (Japan Sigma Koki, Ltd.) is 1×10^{-5}. It can be estimated in advance to modify the measured results. So, the polarization-mixing error can be decreased to $\Delta\phi_p = 0.03°$ with this modification [18].

D. Noises

In practical tests, we have a lot of noises. Because of its common-path optical configuration, two interfering beams travel the same path and they have the same phase noises from the ambient motion. These phase noises will cancel out after interfering and they do not affect the interference signals [19]. So, this method is high stable against the ambient motion. The noises may be electronic noises. To show the validity of our algorithm, different random noise levels from 0 % to 10 % are added to the theoretical digital signals taken by the camera as $\psi = 45°$. Then, they are processed to derive the absolute phases. Their associated phase errors can be calculated and shown in Fig. 8. The abscissa of Fig. 8 means the ratio of the maximum amplitude of the additional random noises to the amplitude of the theoretical signals. We have almost 5 % maximum random noise level in our tests, and we have $\Delta\phi_n = 0.2°$.

Consequently, our total experimental errors are $\Delta\phi = \Delta\phi_0 + \Delta\phi_s + \Delta\phi_p + \Delta\phi_n = 0.3°$. Moreover, this method can be applied to measure two dimensional distributions of the physical quantities which are related to the phase difference between the s- and the p- polarizations, such as the refractive index, the complex refractive index, the (n_e, n_o), the phase retardation,…*etc*. In addition, this method can be modified and applied to the interferometers with a polarization-beam splitter.

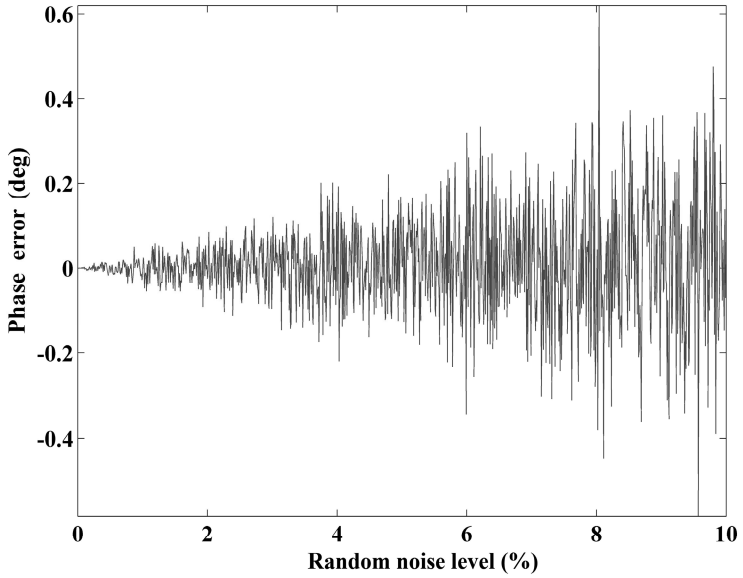

Fig. 8 The relation curves of phase error versus random noise level as $\psi = 45°$.

5. CONCLUSION

An alternative method for full-field absolute phase measurements in the heterodyne interferometer with an electro-optic modulator has been proposed in this paper. An electro-optic modulator is used to introduce a frequency difference between two orthogonal polarizations in the heterodyne interferometer. When the electro-optic modulator is applied with a saw-tooth voltage signal with the amplitude lower than its half-wave voltage, periodical sinusoidal segments are obtained. In the full-field measurements, the segments are taken by a camera and become discrete digital signals. After a series of calculations, the starting point of the sinusoidal segment can be determined accurately. Next, the difference between the period of the saw-tooth signal and that of the periodical sinusoidal segments is inserted into any two neighboring segments. Thus the periodical sinusoidal segments have the same frequency as that of the saw-tooth signal. Then, the periodical sinusoidal segments can be modified as the periodical sinusoidal signals by using a least-square sine fitting algorithm. Subtracting the initial phase of the system from the phase of the periodical sinusoidal signals, the absolute phase measured at the pixel can be obtained. This technique is applied to other pixels, and the full-field absolute phase measurements can be achieved. Its validity has also been demonstrated.

REFERENCES

[1] Massie, N. A., Nelson, R. D. and Holly, S., "High-performance real-time heterodyne interferometry," Appl. Opt. 18, 1797-1803 (1979).

[2] Dandliker, R., Thalmann, R. and Prongue, D., "Two-wavelength laser interferometry using superheterodyne detection," Opt. Lett. 13, 339-341 (1988).

[3] Gelmini, E., Minoni, U. and Docchio, F., "Tunable, double-wavelength heterodyne detection interferometer for absolute-distance measurements," Opt. Lett. 19, 213-215 (1993).

[4] Feng, C. M., Huang, Y. C., Chang, J. G., Chang, M. and Chou, C., "A true sensitive optical heterodyne polarimeter for glucose concentration measurement," Opt. Commun. 141, 314–321 (1997).

[5] Huang, Y. C., Chou, C. and Chang, M., "Direct measurement of refractive Indices of a linear birefringent retardation plate, " Opt. Commun. 133, 11-16 (1997).

[6] Chiu, M. H., Chen, C. D. and Su, D. C., "Method for determining the fast axis and phase retardation of a wave plate, " J. Opt. Soc. Am. A 13, 1924-1929 (1996).

[7] Tkaczyk, T. and Jozwicki, R., "Full-field heterodyne interferometer for shape measurement: experimental characteristics of the system," Opt.Eng. 42, 2391–2399 (2003).

[8] Pitter, M. C., See, C. W. and Somekh, M. G., "Full-field heterodyne interference microscope with spatially incoherent illumination," Opt.Lett. 29, 1200–1202 (2004).

[9] Egan, P., Connely, M. J. and Whelan, M. P., "Random depth access full-field heterodyne low-coherence interferometry utilizing acousto-optic modulation and a complementary metal-oxide semiconductor camera," Opt. Lett. 31, 912–914 (2006).

[10] Akiba, M., Chan, K. P. and Tanno, N., "Full-field optical coherence tomography by two-dimensional heterodyne detection with a pair of CCD cameras," Opt. Lett. 28, 816-818 (2003).

[11] Su, D. C., Chiu, M. H. and Chen, C. D., "Simple two-frequency laser, " Pre. Eng. 18, 161–163 (1996).

[12] IEEE, "Standard for Terminology and Test Methods for Analogto-Digital Converters," IEEE Std 1241-2000, 25-29, Dec. (2000).

[13] Yariv, A., Optical Electronics, Philadelphia, PA: Saunders, W. B., Ch. 9, 309-332 (1991)

[14] Hecht, E., Optics, 4th ed, Addison-Wesley, 376-379 (2002).

[15] Nyquist, H., "Certain topics in telegraph transmission theory," Trans. AIEE 47, 617-644 (1928).

[16] Dou, Q., Ma, H., Jia, G., Chen, Z., Cao, K. and Zhang, T., "Study on measurement of linear electro-optic coefficient of a minute irregular octahedron cBN wafer," Opt. Laser Technol. 39, 647-651 (2007).

[17] Jian, Z. C., Chen, Y. L., Hsieh, H. C., Hsieh, P. J. and Su, D. C., "Optimal Condition for Full-Field Heterodyne Interferometry, " Opt. Eng. 46, 115604 (2007).

[18] Chiu, M. H., Lee, J. Y. and Su, D. C., "Complex refractive-index measurement based on Fresnel's equations and uses of heterodyne interferometry," Appl. Opt. 38, 4047-4052 (1999).

[19] Briers, D., "Interferometric optical testing," in Optical Measurement Techniques and Applications, Rastogi, P. K., ed. (Artech, 1997), pp. 101-103.